# A mean field approach for molecular simulations of fluid systems

Giuseppe Brancato, Alfredo Di Nola, Vincenzo Barone, and Andrea Amadei

Citation: The Journal of Chemical Physics **122**, 154109 (2005); doi: 10.1063/1.1877172
View online: http://dx.doi.org/10.1063/1.1877172
View Table of Contents: http://scitation.aip.org/content/aip/journal/jcp/122/15?ver=pdfcov
Published by the AIP Publishing

# A mean field approach for molecular simulations of fluid systems

Giuseppe Brancato[a)]
*Dipartimento di Chimica, Universitá Federico II, Complesso Monte S. Angelo, Via Cintia, I-80126 Napoli, Italy*

Alfredo Di Nola
*Dipartimento di Chimica, Universitá di Roma "La Sapienza," Piazzale Aldo Moro 5, I-00185 Roma, Italy*

Vincenzo Barone
*Dipartimento di Chimica, Universitá Federico II, Complesso Monte Sant'Angelo, Via Cintia, I-80126 Napoli, Italy*

Andrea Amadei
*Dipartimento di Scienze e Tecnologie Chimiche, Universitá di Roma "Tor Vergata," Via della Ricerca Scientifica 1, I-00133 Roma, Italy*

(Received 15 December 2004; accepted 28 January 2005; published online 20 April 2005)

In this paper we introduce a mean field method for simulating complex molecular systems like liquids and solutions. Using well-established theoretical principles and models, we obtained a relatively simple approach which seems to provide a reliable description of the bulk molecular behavior of liquid water. Moreover, we have applied this approach to study simple solutes in solution, like sodium and chloride ions and acetone. Comparison with standard simulations, performed with periodic boundary conditions, shows that such a mean field method can reproduce the same structural and thermodynamical properties at low computational costs and represents a valid alternative for simulating solute-solvent systems, like solutions of large biomolecules. © *2005 American Institute of Physics*. [DOI: 10.1063/1.1877172]

## I. INTRODUCTION

The development and use of mean field (MF) or implicit solvent methods for simulating realistic molecular systems is continuously increasing.[1–6] MF methods allow, in principle, the correct treatment of molecular systems without the need for simulating an extremely large amount of explicit molecules, and they are very well suited for solute-solvent systems and in particular for the simulation of biological macromolecules. Also, they can be combined with quantum mechanics (QM) and mixed quantum/classical (QM/MM) methods to include inexpensively the solvent contribution (see Ref. 7 and references therein), which is in many cases not negligible, and they could offer significant advantage with respect to periodic boundary conditions (PBC) models to perform *ab initio* molecular dynamics with localized basis sets for the representation of the electronic wave function.[8]

It is worth noting that PBC methodologies, employed in standard simulations, although widely used and efficient can provide unphysical correlations due to the artificial periodicity of the system.[9–16] These correlations are quite negligible, at least for the basic behavior of the system, when solids or homogeneous fluids are considered, but are likely to become more relevant in the case of solute-solvent systems, especially when a polar or charged solute is concerned. Such spurious effects are clearly removed by the use of MF methods, which on the other hand are always affected by explicit boundary effects due to the macroscopic character of the approximations used in the derivation of the MF. However, such boundary effects can be limited when rigorous MFs are used, i.e., based on well sound theoretical principles, and hence for a large assembly of molecules an extended inner part of the simulation box could correctly reproduce the bulk behavior, i.e., the same behavior of an equivalent subpart embedded in a macroscopic system. In this paper we present a MF model, based on well-established theoretical principles, developed for *NVT ensemble* simulations of molecular fluids. In this model we consider the explicit molecules in their simulation box to be embedded in a dielectric continuum. The shape of the simulation box could be quite arbitrary, so that it can be easily adapted to different systems, e.g., a large macromolecule surrounded by solvent molecules. However, because of the mathematical simplicity, in this paper we only consider the special case of a spherical cavity. The MF is composed of three parts: (a) an electrostatic contribution or "reaction field," which accounts for the long-range interactions between the explicit molecules and the dielectric; (b) a van der Waals potential, which represents the short-range dispersion-repulsion interactions, and (c) a rigid boundary surface that keeps the explicit molecules confined in the spherical cavity.

Finally, it is important to remark once again that in this model, as in other MF methods, the approximations used are based on the macroscopic physical behavior and hence they become more reliable as the simulation cavity gets larger.

This paper is organized as follows: In Sec. II, we describe the theoretical and computational details of the MF model and we provide the technical details of the molecular dynamics (MD) simulations performed (Sec. II E). In Sec.

[a)]Electronic mail: brancato@caspur.it

 

III, we compare the results of a set of MD simulations of water using both MF and PBC methods. The same MF model parametrized for pure water has been tested on solute-solvent systems. In particular, we have studied aqueous solutions of sodium and chloride ions (see Sec. III B) and acetone (see Sec. III C). Conclusions are given in Sec. IV.

## II. METHODS

### A. Basic equations

We consider a homogeneous macroscopic *NVT* system where, say in the center, we define a spherical mesoscopic subsystem where we can neglect the density fluctuations as the average number of molecules is rather large. Hence, we can decompose the overall system in two subsystems with fixed volume and number of molecules. Considering a Hamiltonian where no molecular polarization is present, as in a typical simulations, we then have that the (Helmholtz) free energy of a given phase space position of the molecules in the cavity (explicit molecules) is

$$A(\boldsymbol{x}_{\mathrm{I}},\boldsymbol{p}_{\mathrm{I}}) = \mathcal{U}_{\mathrm{I}}(\boldsymbol{x}_{\mathrm{I}},\boldsymbol{p}_{\mathrm{I}}) - kT\ln\left(\Theta^{-1}\int e^{-\beta[\mathcal{V}(\boldsymbol{x}_{\mathrm{I}},\boldsymbol{x}_{\mathrm{II}})+\mathcal{U}_{\mathrm{II}}(\boldsymbol{x}_{\mathrm{II}},\boldsymbol{p}_{\mathrm{II}})]}\frac{d\boldsymbol{x}_{\mathrm{II}}d\boldsymbol{p}_{\mathrm{II}}}{h^{d_{\mathrm{II}}}}\right), \tag{1}$$

where $\boldsymbol{x}_{\mathrm{I}},\boldsymbol{p}_{\mathrm{I}}$ and $\boldsymbol{x}_{\mathrm{II}},\boldsymbol{p}_{\mathrm{II}}$ are the coordinates and conjugated momenta of the mesoscopic subsystem and of the remaining part of the macroscopic *NVT* system (macroscopic subsystem), $\mathcal{U}_{\mathrm{I}}$ and $\mathcal{U}_{\mathrm{II}}$ are the internal energies of the mesoscopic and macroscopic subsystems, $d_{\mathrm{II}}$ is the total number of classical degrees of freedom in the macroscopic subsystem and $h$ is the Planck's constant. Moreover, $\Theta^{-1}$ is a constant providing the quantum correction, $\mathcal{V}$ is the interaction energy between the two subsystems and $\beta^{-1}=kT$ with $k$ the Boltzmann's constant and $T$ the absolute temperature. If in the reference state all the interactions between the two subsystems are set to zero ($\mathcal{V}=0$), we have for the free energy difference,

$$\Delta A(\boldsymbol{x}_{\mathrm{I}},\boldsymbol{p}_{\mathrm{I}}) = A(\boldsymbol{x}_{\mathrm{I}},\boldsymbol{p}_{\mathrm{I}}) - A_{\mathrm{ref}}(\boldsymbol{x}_{\mathrm{I}},\boldsymbol{p}_{\mathrm{I}}) = -kT\ln\left(\frac{\int e^{-\beta[\mathcal{V}(\boldsymbol{x}_{\mathrm{I}},\boldsymbol{x}_{\mathrm{II}})+\mathcal{U}_{\mathrm{II}}(\boldsymbol{x}_{\mathrm{II}},\boldsymbol{p}_{\mathrm{II}})]}d\boldsymbol{x}_{\mathrm{II}}d\boldsymbol{p}_{\mathrm{II}}}{\int e^{-\beta\mathcal{U}_{\mathrm{II}}(\boldsymbol{x}_{\mathrm{II}},\boldsymbol{p}_{\mathrm{II}})}d\boldsymbol{x}_{\mathrm{II}}d\boldsymbol{p}_{\mathrm{II}}}\right), \tag{2}$$

which is also known as the "potential of mean force" or shortly the "mean field" (MF), $W(\boldsymbol{x}_{\mathrm{I}})\equiv\Delta A(\boldsymbol{x}_{\mathrm{I}},\boldsymbol{p}_{\mathrm{I}})$. This is the potential field experienced by the explicit molecules in a given configuration due to the average interactions with the environment. Continuum models differ in the way $W$ is approximated.[1–3]

According to commonly used force fields for computer simulations (e.g., GROMOS,[17] AMBER,[18] CHARMM[19]), the nonbonded interactions can be separated into long-range electrostatic and short-range van der Waals contributions. The latter accounts for the dispersion and repulsive interactions. By using this decomposition we have

$$\mathcal{V}(\boldsymbol{x}_{\mathrm{I}},\boldsymbol{x}_{\mathrm{II}}) = \mathcal{V}_{\mathrm{elec}}(\boldsymbol{x}_{\mathrm{I}},\boldsymbol{x}_{\mathrm{II}}) + \mathcal{V}_{\mathrm{vdW}}(\boldsymbol{x}_{\mathrm{I}},\boldsymbol{x}_{\mathrm{II}}). \tag{3}$$

Consequently, we can define two corresponding terms for $W(\boldsymbol{x}_{\mathrm{I}})$:

$$W(\boldsymbol{x}_{\mathrm{I}}) = W_{\mathrm{elec}}(\boldsymbol{x}_{\mathrm{I}}) + W_{\mathrm{vdW}}(\boldsymbol{x}_{\mathrm{I}}), \tag{4}$$

where

$$W_{\mathrm{elec}}(\boldsymbol{x}_{\mathrm{I}}) = -kT\ln\left(\frac{\int e^{-\beta[\mathcal{V}_{\mathrm{elec}}+\mathcal{U}_{\mathrm{II}}]}d\boldsymbol{x}_{\mathrm{II}}d\boldsymbol{p}_{\mathrm{II}}}{\int e^{-\beta\mathcal{U}_{\mathrm{II}}}d\boldsymbol{x}_{\mathrm{II}}d\boldsymbol{p}_{\mathrm{II}}}\right), \tag{5}$$

$$W_{\mathrm{vdW}}(\boldsymbol{x}_{\mathrm{I}}) = -kT\ln\left(\frac{\int e^{-\beta[\mathcal{V}_{\mathrm{elec}}+\mathcal{V}_{\mathrm{vdW}}+\mathcal{U}_{\mathrm{II}}]}d\boldsymbol{x}_{\mathrm{II}}d\boldsymbol{p}_{\mathrm{II}}}{\int e^{-\beta[\mathcal{V}_{\mathrm{elec}}+\mathcal{U}_{\mathrm{II}}]}d\boldsymbol{x}_{\mathrm{II}}d\boldsymbol{p}_{\mathrm{II}}}\right). \tag{6}$$

### B. Electrostatic term (reaction field)

Generally, the electrostatic contribution, $W_{\mathrm{elec}}$, is derived from macroscopic continuum theory.[1,2] Given a molecular charge distribution enclosed in a cavity of a dielectric medium, the electric potential is obtained from the Poisson equation,[20]

$$\Delta[\epsilon(\boldsymbol{r})\Delta\Phi(\boldsymbol{r})] = -4\pi\rho_{\mathrm{I}}(\boldsymbol{r}), \tag{7}$$

where $\Phi(\boldsymbol{r})$ is the electrostatic potential at point $\boldsymbol{r}$, $\rho_{\mathrm{I}}(\boldsymbol{r})$ represents the molecular charge density and $\epsilon(\boldsymbol{r})$ is the position-dependent dielectric constant. $W_{\mathrm{elec}}$ can be considered as the reversible work needed to charge the explicit molecules in the dielectric cavity. It can be shown that

$$W_{\mathrm{elec}}(\boldsymbol{x}_{\mathrm{I}}) = \sum_i\int_0^{e_i}\Phi_{\mathrm{RF}}(\boldsymbol{r}_i)de_i' = \frac{1}{2}\sum_i e_i\Phi_{\mathrm{RF}}(\boldsymbol{r}_i), \tag{8}$$

where $e_i$ is the $i$th atomic partial charge and $\Phi_{\mathrm{RF}}(\boldsymbol{r}_i)$ is the electric potential at the atomic site $\boldsymbol{r}_i$ only due to the macroscopic subsystem, which implicitly depends on the charges $e_i$. $\Phi_{\mathrm{RF}}(\boldsymbol{r}_i)$ is the so-called "reaction field" potential, that is the electric field generated by the polarization of the dielectric continuum induced by the molecular charge distribution. Since the works of Bell[21] and Onsager[22] in the 1930s, many different approaches have been developed to describe this phenomenon.[23,24] Within the continuum approximations, the reaction field and its potential can be expressed analytically using the multipole expansion of the charge distribution[20] and the generalized Born theory[25] or numerically by solving the Poisson equation with either the finite difference method[26,27] or the boundary element (BE) method.[28–31]

Although for the special case of a spherical cavity as well as for other regular cavities an analytical solution of $\Phi_{\mathrm{RF}}(r_i)$ based on multipole expansion of the charge distribution exists, in this work we have used a more flexible BE method, which is based on the polarizable continuum model (PCM) approach.[28,32] The details of this methodology can be found elsewhere.[32] Briefly, it consists on partitioning the cavity surface in small elements called tesserae, which have typically a triangular shape, of approximately equal areas and then determining the "apparent surface charges," $q_{\mathrm{asc}}$, centered on each tessera for a given charge distribution of the explicit molecules. The computation of $q_{\mathrm{asc}}$ requires the solution of a system of $N_{\mathrm{tes}}$ linear equations,

$$\boldsymbol{D}\cdot\boldsymbol{q}_{\mathrm{asc}} = -\boldsymbol{E}_{\boldsymbol{m},\perp} \tag{9}$$

with

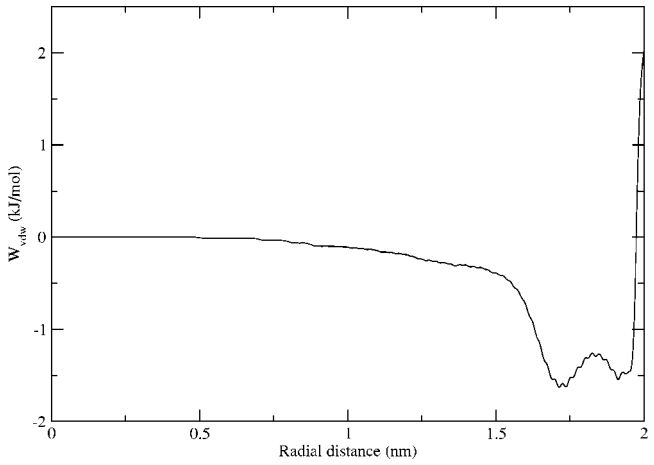


FIG. 1. van der Waals potential determined for a spherical box of SPC water at ambient conditions ($\rho$=55.32 mol/l; $T$=300 K).

$$\boldsymbol{E}_{\boldsymbol{m},\perp}(\boldsymbol{s_i}) = \boldsymbol{E_m}(\boldsymbol{s_i}) \cdot \boldsymbol{n}(\boldsymbol{s_i}), \tag{10}$$

where $\boldsymbol{s_i}$ is the position vector of the $i$th tessera, $\boldsymbol{n}(\boldsymbol{s_i})$ is the corresponding normal vector pointing outward the cavity, $\boldsymbol{E_m}$ is the electric field only due to the molecular charges, $\boldsymbol{q}_{\text{asc}}$ is the array of the "apparent surface charges," and $\boldsymbol{D}$ is a matrix that depends only on the surface topology and on the dielectric constant,

$$D_{ii} = \frac{\mathbf{1}}{a_i}\left[\frac{4\pi\epsilon}{\epsilon - 1} - \sum_{j\neq i} D_{ji}a_j\right], \tag{11}$$

$$D_{ij} = \frac{(\boldsymbol{s_i} - \boldsymbol{s_j}) \cdot \boldsymbol{n_i}}{|\boldsymbol{s_i} - \boldsymbol{s_j}|^3}, \tag{12}$$

where $a_i$ is the area of the $i$th tessera and $\epsilon$ is the continuum dielectric constant. This is an accurate approximation in the limit of a macroscopic cavity and an infinite number of tesserae ($N_{\text{tes}} \to \infty$).

In this work, a spherical cavity of radius 2.0 nm has been used to confine the explicit molecules, as described in Sec. II D. Consequently, the dielectric continuum radius, $R_c$, which is the distance where the dielectric begins, has been optimized in order to reproduce correctly bulk properties of water ($R_c$=2.188 nm). Also, we have found that $N_{\text{tes}}$=1500 is a good compromise between efficiency and accuracy, corresponding to an average tessera area of 4.0 Å$^2$. We did not observe significant differences in our results with a much larger number of tesserae ($N_{\text{tes}}$=3840). The cavity surface has been partitioned using an improved GEPOL procedure.[33]

Finally, it should be noted that Eq. (9) can be solved by inverting the $\boldsymbol{D}$ matrix only once at the beginning of the simulation and then by recomputing at each step the electric field due to the molecular system.

### C. van der Waals term

The dispersion-repulsion or van der waals (VdW) term, $W_{\text{vdW}}$, has been determined empirically using a new methodology from a test simulation of liquid water, in this case SPC[34] water (see details in Sec. II E). As a result, the form of the VdW potential (see Fig. 1) depends on the specific molecular system and thermodynamic conditions adopted in this study. Nevertheless, we think that our approach can be easly extended to derive $W_{\text{vdW}}$ potentials for a large number of solvents at different physical conditions, i.e., density, pressure, and temperature. The idea of our method is somehow inspired by the approach of Laio and Parrinello[35] to estimate the free energy surface of a complex many-body system. First, we have assumed that the potential $W_{\text{vdW}}(r)$ is a radial function acting on each explicit water molecule embedded in the cavity and, in particular, on the oxygen atoms according to the SPC model, which has a Lennard-Jones site centered on the oxygen. Second, we have expressed $W_{\text{vdW}}(r)$ as the sum of a set of $N_g$ Gaussian functions, $g_i$, whose centers, $r_i$, are equally spaced over a radial direction of the spherical cavity,

$$W_{\text{vdW}}(r) = \sum_i g_i(r - r_i) = \sum_i \lambda_i \exp\left(-\frac{(r - r_i)^2}{2\sigma^2}\right). \tag{13}$$

Each $g_i(x)$ function has the same spread, $\sigma$, but a different height, $\lambda_i$, which is a multiple of a fixed amount ($\lambda_i = n_i h$). During the test simulation, the Gaussian heights are allowed to change in order to keep constant the local density of the liquid to its overall value, $\rho(r_i) = \rho_0$.

The method works as follows: after a certain time interval, $\tau$, the local densities $\rho(r_i)$ are computed and their values compared to the constant overall density $\rho_0$. If $\rho(r_i) > \rho_0$, the corresponding Gaussian height is increased by one unit $h$ ($n_{i,\text{new}} = n_{i,\text{old}} + 1$), otherwise, if $\rho(r_i) < \rho_0$, the height is decreased ($n_{i,\text{new}} = n_{i,\text{old}} - 1$). In few nanoseconds the $W_{\text{vdW}}(r)$ potential converges to an optimal form, that is, it does not change significantly anymore. To obtain a reliable $W_{\text{vdW}}(r)$ function in an efficient manner, care should be taken in the choice of the Gaussian parameters $N_g$, $\sigma$, and $h$. In this work, we have obtained $W_{\text{vdW}}$ from a 4 ns simulation, updating the Gaussian height, $\lambda_i$, every 20 ps and performing an average

TABLE I. Simulation conditions and input parameters.

| | No. molecules | Box(type; dimension) | Long-range int | $\epsilon_r^{\text{ext}}$ |
|---|---|---|---|---|
| MF | 1116 | Sphere; 2.0 nm (radius) | All pairs | 78 |
| Cutoff | 2180 | Cubic; 4.021 86 nm | 1.5 nm[a] | ⋯ |
| GRF | 2180 | Cubic; 4.021 86 nm | 1.5 nm+RF[b] | 78 |
| PME | 2180 | Cubic; 4.021 86 nm | Grid 35×35×35; Fourth order[c] | ∞ |
| PME2 | 7280 | Cubic; 6.023 3 nm | Grid 52×52×52; Fourth order[c] | 70 |

[a]Radius of cutoff.
[b]Radius of cutoff plus reaction field (RF).
[c]Number of grid points; order of spline functions.

over the last 2 ns. We have found that $N_g=80$, $\sigma=0.0125$ nm, and $h=0.01$ kJ/mol are appropiate values for the liquid system considered.

### D. Boundary treatment

The treatment of the cavity boundaries, rather than general, is to be regarded as an ad hoc method satisfying two main requirements: (1) keeping the molecules confined into a spherical cavity of fixed radius and (2) moderating the unwanted boundary effects that any physical surface necessarily implies. Also, it should be noted that the method proposed is the result of an optimization process for simulations of SPC water at normal conditions and hence, different choices could be more appropriate for other molecular systems and/or physical conditions, e.g., density and temperature. The confinement is realized by means of a rigid cavity surface, with a radius of $R_s=2.0$ nm, on which molecules undergo elastic collisions. The trajectory of a colliding molecule is then modified with respect to its center of mass motion to avoid any effect on the molecular rotational motions. Inside the cavity, 1116 SPC water molecules have been placed, corresponding to a density of $\rho=55.32$ mol/l. Note that the presence of this "constraint" will not alter the statistical mechanical consistency of the whole system as defined in the previous sections.

Other options were examined to avoid strong deviations from the bulk behavior close to the cavity boundary, such as the use of multiple rigid surfaces that keep trapped the outer layers of molecules or the addition of a surface tension term to the mean field. However, the proposed solution gave the most satisfactory results and, besides, we observed that the properties of the inner part of the molecular system are not really affected by a different treatment of the boundaries.

### E. Simulation details

A set of *NVT* molecular dynamics simulations ($\rho=55.32$ mol/l; $T=300$ K) of SPC[34] water were performed using the MF model and three periodic boundary conditions methodologies. The latter are: a method based on simple cutoff radius (Cutoff), a generalized reaction field (GRF),[36] and a particle-mesh Ewald method (PME)[37] (see Table I for details). The dielectric constant of the external medium in GRF and PME simulations, $\epsilon_r^{\text{ext}}$, was chosen in agreement with the values reported in literature: 78 for GRF and infinite for PME. An additional PME simulation (PME2) with $\epsilon_r^{\text{ext}}=70$, which is the relative dielectric constant as obtained by PME simulation of SPC water (see Sec. III A) was also performed. For the MF simulations, we have chosen $\epsilon_r^{\text{ext}}=78$. All simulations are 10 ns long. Furthermore, aqueous solutions of Na and Cl ions and acetone have been studied with MF model (using the same cavity size), and GRF (ions) and PME (acetone). In particular, three charge states, $q=0.0$, $q=0.5$, and $q=1.0$, for Na and two, $q=-0.5$ and $q=-1.0$, for Cl have been examined.

All simulations have been performed, in double precision, with a modified version of the GROMACS[38] simulation package, which includes, for the purpose of this work, the MF model and the Gaussian isokinetic thermostat.[39] Also, the GROMACS[38] force field has been adopted with the exception of the acetone intra and intermolecular potentials.[40]

## III. RESULTS AND DISCUSSION

### A. Pure water

Here we present the results of a comparative study on liquid water between MF and PBC methods. We have adopted the SPC water model at the typical liquid density and temperature, but it should be noted that the MF approach is not limited to a specific molecular model and could also be implemented in *ab initio* molecular dynamics.

In the following, physical properties are evaluated globally as well as locally, in order to show the effect of different boundary conditions. In the latter case, we have extracted inner spherical regions of growing dimension, starting from the center of the simulation box.

First, we have examined the average local density and the molecular dipole orientation in the MF simulation. In general, deviations from liquid bulk behavior are expected only in proximity of the physical boundaries. In Fig. 2, the

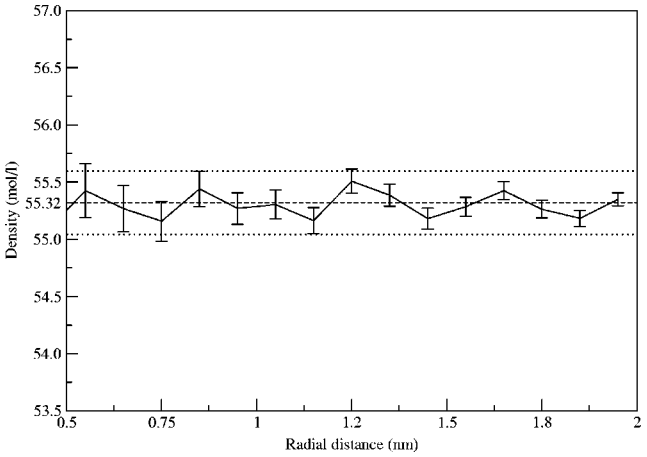


FIG. 2. Average local density. The horizontal dashed line is the density of the overall system (55.32 mol/l) and the two dotted lines indicate a deviation of 0.5%. Error bars correspond to a single standard deviation.

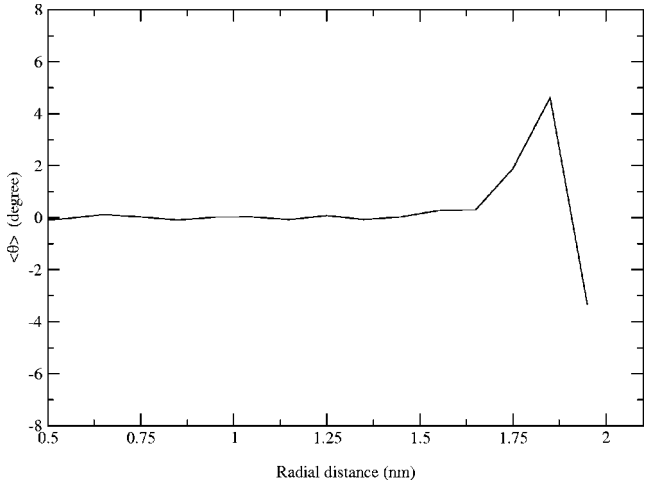


FIG. 3. Average molecular orientation with respect to the radial direction. $\langle\theta\rangle=0°$ corresponds to a completely random orientation.

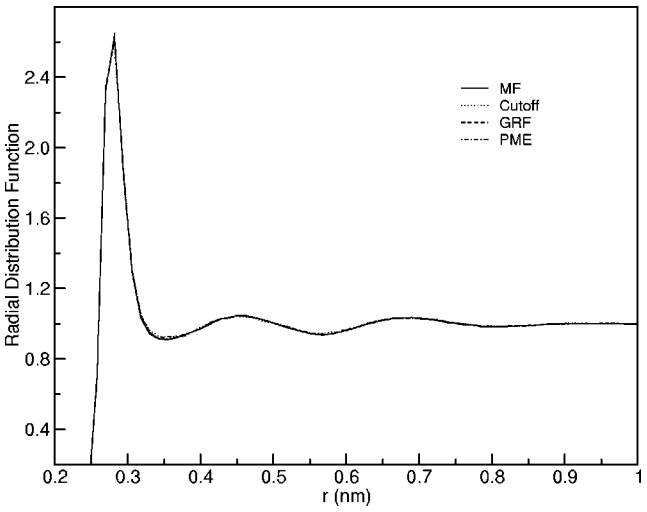


FIG. 4. Oxygen–oxygen radial distribution functions of water.

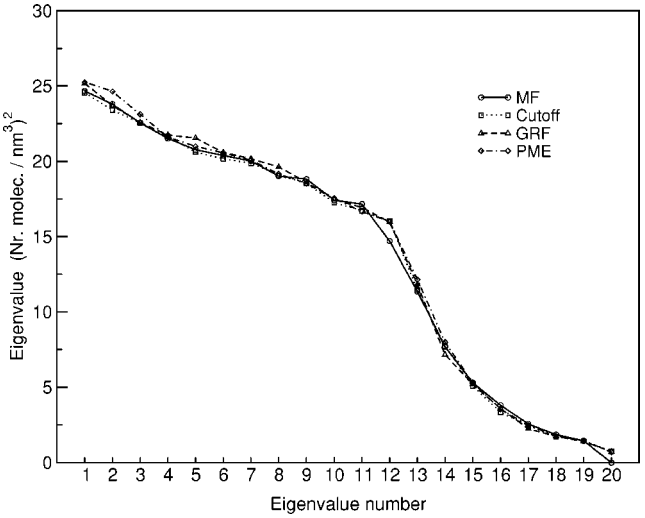


FIG. 5. Eigenvalues of the spatial density covariance matrix built from 20 concentric spherical layers up to a radius of 2.0 nm.

average local density computed in spherical layers of 1 Å width is reported. It is evident that the density is within the statistical errors equal to the overall density (55.32 mol/l), and in any case the deviations are smaller than 0.5%. This result supports the effectiveness of the $W_{\mathrm{vdW}}$ potential in moderating the unwanted boundary effects on the solvent. Another effect due to the spherical boundaries, which is more relevant for a strongly associative liquid like water, is a partial reorientation of the outer molecules with respect to a radial direction: the tendency to form a favorable hydrogen-bonding pattern results in a not completely random orientation of the molecules close to the boundaries. The average angle, $\langle\theta\rangle$, between the water molecular dipole and the radial distance vector pointing to the molecule center of mass from the center of the cavity is plotted in Fig. 3. It is clear that the deviations from the optimal behavior ($\langle\theta\rangle=0°$) are quite limited and $\langle\theta\rangle$ reaches a maximum value of about 4°.

Our comparison of the four methodologies (MF, Cutoff, GRF, PME) starts by considering a structural property, such as the radial distribution function. We have observed virtually identical oxygen-oxygen RDFs in all cases (see Fig. 4), which means that structural properties are almost independent of the treatment of long-range interactions. Also, we have analyzed the spatial density correlations via the covariance matrix of the density fluctuations for 20 concentric spherical layers and, by its diagonalization, the corresponding eigenvalues have been computed and are reported in Fig. 5. The layers are chosen with the same volume (approximately the same average number of molecules) up to a radius of 2.0 nm. All the different simulations provide a good general agreement. Note that the last eigenvalue of the MF simulation is zero because of the constraint on the total number of molecules. In Fig. 6, the normalized autocorrelation function of the molecular dipole moment is reported. Within the statistical errors, which are omitted in the plot for clarity, the same behavior is observed with the exception of the Cutoff simulation.

In order to compare the different simulation methods and to understand the reliability of the MF approach proposed, we have evaluated other typical properties such as the average molecular potential energy (molecular excess internal energy), $U_{\mathrm{pot}}$, the molecular heat capacity (molecular excess heat capacity), $C_V$, the diffusion coefficient, $D$, and the internal dielectric constants, $\epsilon_r^{\mathrm{int}}$, as obtained from total dipole fluctuations.[41] The results for all methods are summarized in Table II. The effect of the mean field is taken into account exactly in $U_{\mathrm{pot}}$, i.e., including the average interactions between the explicit molecules and the dielectric outside the cavity. $C_V$ has been computed via the fluctuations of $U_{\mathrm{pot}}$, which is a physically rigorous method for PBC simulations and just an approximation for MF. Nevertheless, we think that such an approximation is negligible compared to the statistcal noise.

The excess internal energies are comparable as reported in Table II, showing a higher energy for Cutoff, −42.2, and a smaller energy for MF, −40.4, with respect to GRF (−41.6) and PME (−41.5) which are almost equal. The MF result is mainly affected by the approximations in the computation of the reaction field free energy, $W_{\mathrm{elec}}$, as stated in Sec. II B. Briefly, the short-range interactions between the explicit molecules close to the boundary and the dielectric continuum are

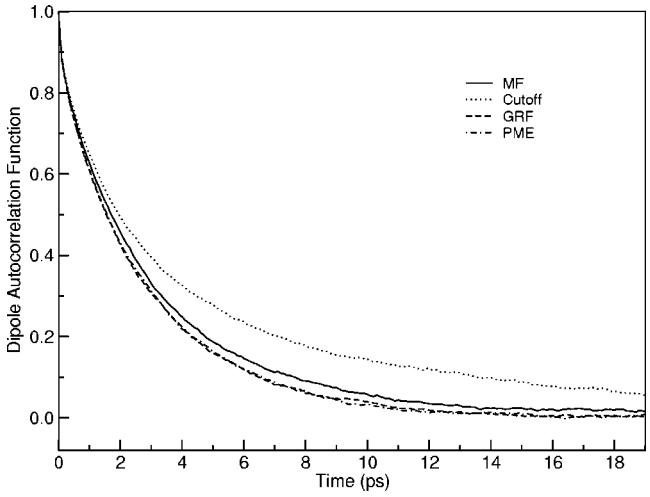


FIG. 6. Molecular dipole moment autocorrelation functions.

TABLE II. Thermodynamic properties of water.

| | $U_{pot}$[a] (kJ/mol) | $C_V$[b] (J/mol K) | $D$[c] ($10^{-5}$ cm$^2$/s) | $\epsilon_r^{intd}$ |
|---|---|---|---|---|
| MF | −40.4 | 55.6±2 | 4.3 | 69.1±2.0 |
| Cutoff | −42.2 | 54.4±2 | 4.4 | 43.0±18 |
| GRF | −41.6 | 51.2±2 | 4.5 | 67.3±2.0 |
| PME | −41.5 | 50.1±2 | 4.3 | 69.2±2.0 |

[a]The average molecular potential energy.
[b]Molecular heat capacity.
[c]Diffusion constant.
[d]The internal dielectric constants.

underestimated to some degree. An higher energy value, in agreement with GRF and PME, can be obtained by increasing the number of tesserae partitioning the cavity surface at the expense of a greater computational effort. However, it is worth to note that a value of −41.5 is obtained if we consider an internal region of radius 1.8 nm, that is, excluding the first most external water layer.

Also, the excess heat capacities, $C_V$, show a reasonable agreement for all methods. Note that the same property evaluated as derivative of the temperature gives a value of 54.7 J/mol K for MF, which is not different from 55.6 within the statistical errors, and supports the internal consistency of this methodology. We have observed a very similar mobility of the water molecules in all simulations, as shown by the diffusion constant values. Remarkably, the diffusion constant of MF computed from the overall system, $D=4.3$, agrees well with that evaluated only in an outer region of the cavity between 1.6 and 2.0 nm, $D=4.5$, which means that the dynamical behavior of water is homogeneous throughout the whole spherical box.

The dielectric constants, $\epsilon_r^{int}$, as derived from the dipole moment fluctuations,[41] are reported on the last column of Table II. It should be noted that in the case of MF, $\epsilon_r^{int}$ depends somewhat on the definition of the volume which encloses all the explicit charges, not just the center of mass of the water molecules. For such a reason, we decided to use simply the volume of a sphere of radius 2.0964 Å, which corresponds to the largest distance observed during the entire simulations by an atom from the center of the cavity. In any case, we are confident that other possible choices of this volume will not lead to a deviation from the reported value (69.1) larger than the statistical error. As expected, the Cutoff value, 43.0, is unrealistic, due to the approximations involved in such a model, whereas GRF (67.3) and PME (69.2) give similar results to previous studies[42–44] and agree quite well with MF value, 69.1.

Finally, the local dipole fluctuations per molecule are plotted against the distance from the center of the box in Fig. 7. Note that the data refer to subsystems contained in spherical regions of increasing radius, and not in spherical layers as used previously. Cutoff results are again completely meaningless and, hence, are omitted for clarity. The use of GRF improves the regularity of the plot, but the values obtained are significantly lower than MF and PME, and are approximately constant in the range between 0.6 and 1.4 nm. The MF model provides an initial increase of the dipole fluctuations, followed by a range (from about 1.2 to 1.8 nm) where the curve is basically flat within the statistical noise. Finally, significant deviations are observed when the molecules belonging to the outer layers are included in the statistics. In particular, the lack of short-range interactions decreases dramatically the friction between molecules and, as a result, the dipole fluctuations are considerably enhanced. In the case of

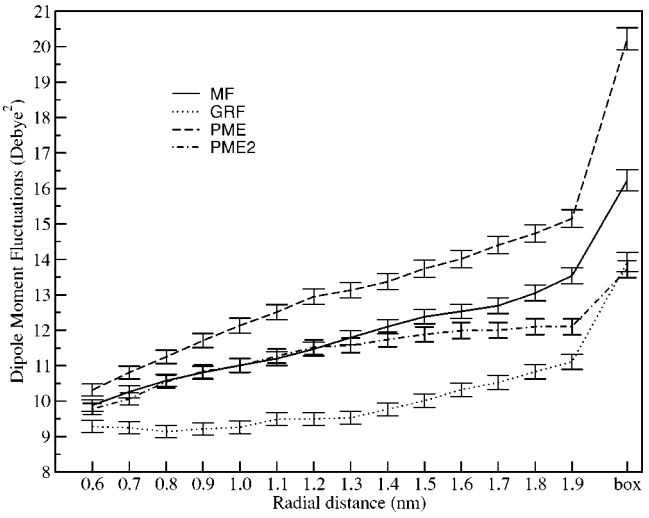


FIG. 7. Dipole moment fluctuations per molecule. The values refer to average fluctuations computed in spherical region of increasing size. Last points (box) are the overall dipole moment fluctuations. Error bars correspond to a single standard deviation.

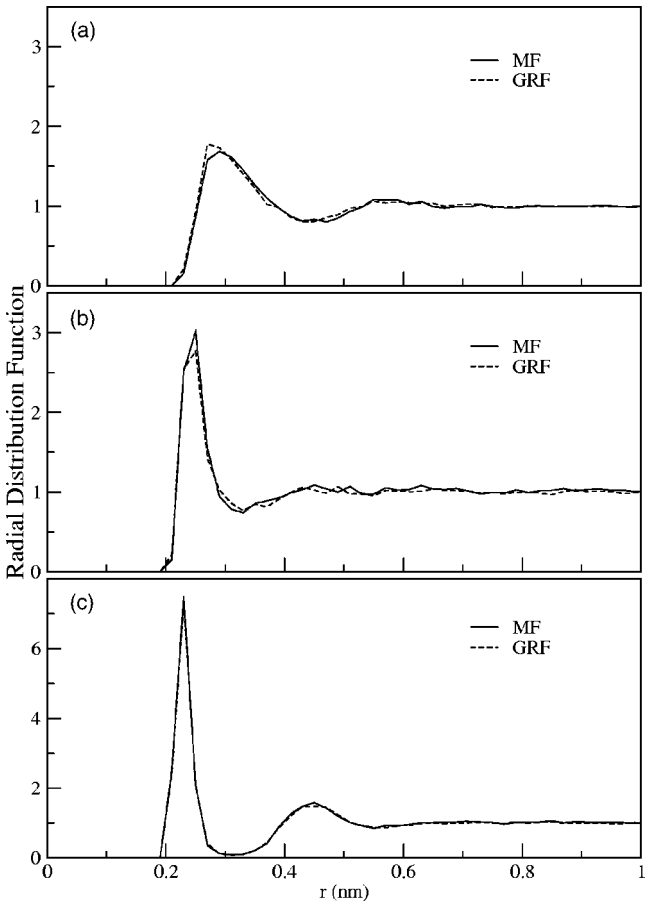


FIG. 8. Sodium–oxygen radial distribution functions. The sodium ion charge is: (a) $q(\mathrm{Na})=0.0$, (b) $q(\mathrm{Na})=0.5$, and (c) $q(\mathrm{Na})=1.0$.

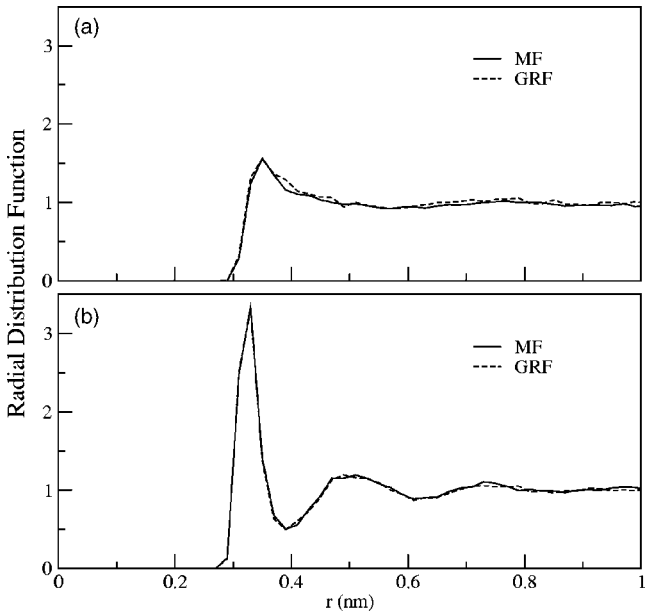


FIG. 9. Chloride–oxygen radial distribution functions. The chloride ion charge is: (a) $q(\mathrm{Cl})=-0.5$ and (b) $q(\mathrm{Cl})=-1.0$.

PME, we observe a similar initial trend, though no apparent plateau, as seen in the MF simulation, is present. Instead, the dipole fluctuations increase monotonically until all the box is considered (last point). Such a behavior could be the effect of the external dielectric medium, which virtually acts as a conductor because of $\epsilon_r^{\mathrm{ext}}$ is set to infinite. In such conditions, both the global and, consequently, the local dipole fluctuations are enhanced. Two possible alternatives can be followed to deal with this problem. One is to enlarge the box such as the local properties can be regarded as indistinguishable from those of a macroscopic liquid system. The second is to set a finite dielectric constant for the external medium. As a compromise, we performed a simulation of a larger system (PME2), with 7280 molecules and 6.0233 nm edge, and we set the value of $\epsilon_r^{\mathrm{ext}}=70$, which roughly corresponds to the dielectric constant previously obtained with PME (see the last column in Table II). In this new PME simulation, the calculated dielectric constant, 68.8, is, within the statistical noise, the same as the previous PME value (69.2) and, as expected, it is not affected by the change of $\epsilon_r^{\mathrm{ext}}$. On the other hand, the plot of the dipole fluctuations is in very good agreement with MF, as reported in Fig. 7, at least up to 1.8 nm: it shows the same plateau from about 1.2 nm. This result suggests that the external medium can influence significantly the internal local dipole fluctuations as well as the system size. Further, it is worth noting that the global dipole fluctuations value for PME2, 13.6 $\mathrm{D}^2$, is higher than the plateau value, 12.0 $\mathrm{D}^2$. Such a discrepancy could be determined by the limited size of the simulation box as well as by the long range correlation effects due to the periodicity of the model. However, further studies are necessary to clarify this point.

### B. Ion solutions

The MF model parametrized for pure water as described in Sec. II has been applied to study aqueous solutions of sodium and chloride ions at ambient conditions. In particular, we have performed three simulations of the Na–water system with different ion charges, $q(\mathrm{Na})=0.0$, $q(\mathrm{Na})=0.5$, $q(\mathrm{Na})=1.0$, and two Cl–water simulations with $q(\mathrm{Cl})=-0.5$ and $q(\mathrm{Cl})=-1.0$. In all cases, the ion position has been fixed at the center of the spherical cavity. In order to compare MF results with standard PBC methods we have simulated the same systems using the generalized reaction field (GRF) method. In Figs. 8 and 9, the Ion$-\mathrm{O}_{\mathrm{wat}}$ radial distribution functions are reported for both MF and GRF. As expected, the structural properties are not affected by the choice of the MD boundary conditions and all the simulations give very similar results. Furthermore, we have examined the ion solvation energy by computing the intermolecular interactions between the ion and the explicit water molecules contained in a sphere of radius 2.0 nm centered at the ion position. In Table III, we report the density $\rho$ $((N_{\mathrm{wat}}+1)/V)$, the electrostatic potential $\phi$ with its fluctuations $\sigma^2(\phi)$, and the Lennard-Jones interaction energy $U_{lj}$. Note that the density is fixed for MF simulations, e.g., all water molecules are involved in the calculations, whereas it can slightly vary for GRF, where a spherical sample is extracted from the rectangular box. Also, we have neglected the mean field contributions to $\phi$ and $U_{lj}$, in such a way to compare these properties

TABLE III. Comparison between MF and PBC results for sodium and chloride ion solutions. $\rho$ $((N_{\mathrm{wat}}+1)/V)$, $\phi$, $\sigma^2(\phi)$, and $U_{lj}$ are, respectively, the density, the electrostatic potential at the ion site, the fluctuations and the Lennard-Jones ion-water interaction energy. All results refer to a subsystem included in a spherical region of radius 2.0 nm centered at the ion site. The estimated errors from block averages for $\phi$, $\sigma^2(\phi)$, and $U_{lj}$ are, respectively, 5, 100, and 0.3.

| Solute | Charge ($e$) | Method | $\rho$ ($\mathrm{nm}^{-3}$) | $\phi$ (kJ/mol $e$) | $\sigma^2$ ($\phi$) | $U_{lj}$ (kJ/mol) |
|---|---|---|---|---|---|---|
| Na | 0.0 | MF | 33.273 | −20.9 | 1990 | −0.16 |
| Na | 0.0 | GRF | 33.343 | −32.2 | 1990 | 0.2 |
| Na | 0.5 | MF | 33.273 | −414.8 | 2170 | 11.8 |
| Na | 0.5 | GRF | 33.353 | −425.5 | 2600 | 12.2 |
| Na | 1.0 | MF | 33.273 | −865.8 | 2200 | 47.8 |
| Na | 1.0 | GRF | 33.374 | −868.9 | 2240 | 46.3 |
| Cl | −0.5 | MF | 33.273 | 280.5 | 2020 | −1.8 |
| Cl | −0.5 | GRF | 33.290 | 267.7 | 2010 | −1.8 |
| Cl | −1.0 | MF | 33.273 | 660.6 | 1910 | −2.3 |
| Cl | −1.0 | GRF | 33.312 | 635.1 | 2060 | −2.2 |

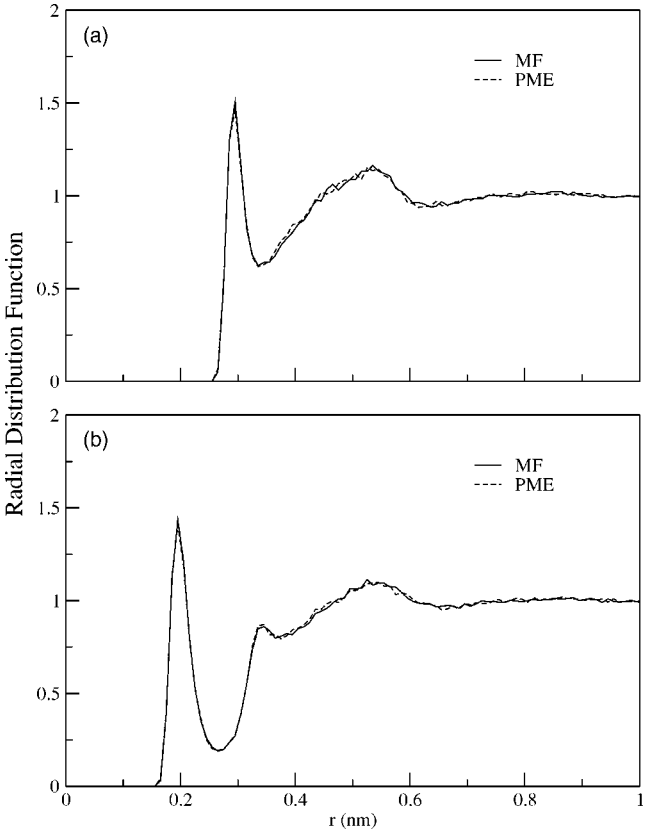


FIG. 10. (a) $O_{act}-O_{wat}$ and (b) $O_{act}-H_{wat}$ radial distribution functions.

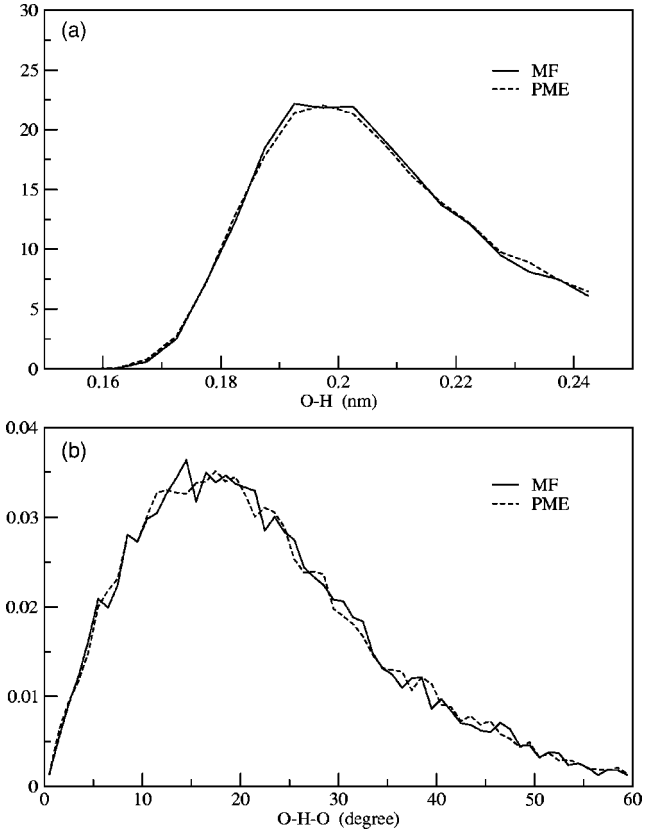


FIG. 11. (a) $O_{act}-H_{wat}$ hydrogen bond distance distributions and (b) $O_{act}-H_{wat}-O_{wat}$ hydrogen bond angle distributions.

TABLE IV. Comparison between MF and PME results for an aqueous solution of acetone. $\rho$ $((N_{wat}+1)/V)$, $U_{el}$ and $\sigma^2(U_{el})$ are, respectively, the density, the acetone-water electrostatic energy and its fluctuations, and refer to a subsystem included in a spherical region of radius 2.0 nm centered at the acetone carbonylic carbon. $\langle\mu\rangle$ is the acetone dipole moment and $N_{hb}$ is the average number of hydrogen bonds. The estimated errors from block averages for $U_{el}$ and $\sigma^2(U_{el})$ are, respectively, 0.4 and 6.

| | $\rho$ ($nm^{-3}$) | $U_{el}$ (kJ/mol) | $\sigma^2$ ($U_{el}$) | $\langle\mu\rangle$ (D) | $N_{hb}$ |
|---|---|---|---|---|---|
| MF | 33.184 | −49.1 | 223 | 4.85 | 2.14 |
| PME | 33.240 | −47.5 | 242 | 4.85 | 2.13 |

consistently. We observe an overall good agreement between MF and GRF results within the statistical errors. The deviations in $\sigma^2(\phi)$ are probably due to the slowly convergent behaviour of this property.

### C. Acetone

The MF model has also been used in a simulation of an aqueous solution of acetone, as a test model for a more complex solute. The acetone molecule was placed at the center of a spherical cavity of the same dimension seen above and solvated with 1111 SPC water molecules $((N_{wat}+1)/V = 33.184\ nm^{-3})$. The roto-traslation motions of the solute have been removed during the dynamics using the method described in Ref. 45. Analogously, we have performed a simulation of the same system in periodic boundary conditions with PME method. In Fig. 10, the $O_{act}-O_{wat}$ and $O_{act}-H_{wat}$ RDFs are reported for comparison: the results for MF and PME are practically undistinguishable. Also, a very good agreement has been observed in the hydrogen bonding arrangement between the carbonyl group and water as shown by the $O_{act}-H_{wat}$ distance distribution [Fig. 11(a)], the $O_{act}-H_{wat}-O_{wat}$ angle distribution [Fig. 11(b)] and the average number of hydrogen bonds, $N_{hb}=2.14$ (MF) and $N_{hb}=2.13$ (PME). All these results along with a very similar acetone geometry conformation (results not shown) confirm that the structural properties of the solute-solvent system seem to be unchanged.

In Table IV, we report the average density, $\rho$ $((N_{wat}+1)/V)$, the acetone–water electrostatic energy, $U_{el}$, with its fluctuations, $\sigma^2(U_{el})$, the acetone dipole moment and the number of hydrogen bonds, $N_{hb}$. Note that, similar to what was seen in the previous section, both energy and density refer to a spherical region of radius 2.0 nm centered at the carbonylic carbon atom. No reaction field term has been added to $U_{el}$ and $\sigma^2(U_{el})$. All the results show a remarkable agreement and support the use of the MF model in treating solute-solvent systems.

## IV. CONCLUSIONS

In this work, the use of a mean field based approach (MF) has been exploited to perform molecular dynamics simulations of liquid water and simple aqueous solutions. To this end, charged solutes, like sodium and chloride ions, and a strongly dipolar molecule, like acetone, have been studied as test systems at ambient conditions.

The results on water suggest that liquid bulk properties can be well reproduced with the MF model: the comparison of structural properties, mobility and typical thermodynamical properties, like the excess energy and heat capacity, shows a very good agreement between MF and commonly used PBC methods, with the exception of Cutoff, which completely neglects an important part of the long-range intermolecular interactions. Also, the analysis of the local density, molecular orientation distribution, and the spatial density correlations demonstrate that the MF method can effectively reduce the unwanted boundary effects, which are in principle present whenever a physical confinement is introduced in a simulation.

Furthermore, investigation of the local dipole fluctuations, evaluated on subsystems of growing dimension, revealed more noticeable differences between the models considered: only PME and MF have shown the best agreement, which not surprisingly are the two more rigorous methods from a statistical mechanical point of view. As expected, PME results are greatly affected by the choice of the dielectric constant of the external medium, which also means that some care should be adopted in using this methodology. Remarkably, all methods have comparable computational costs.

Besides, the study of simple solute-solvent systems with MF, without any reparametrization of the model, and the corresponding comparison with PBC simulations have shown the reliability and flexibility of the method proposed in this paper.

It has to be pointed out that the present MF model can be extended to perform constant pressure simulations. We expect that MF can be fruitfully used for simulating complex molecular systems and, especially, solution of large macromolecules where the number of solvent molecules can be conveniently reduced without the loss of a physically rigorous treatment of the long-range interactions.

## ACKNOWLEDGMENTS

The authors thank CASPUR (Rome) and BioTekNet (Naples) for computer facilities. G.B. is pleased to thank Dr. Giovanni Chillemi of CASPUR for many suggestions regarding the simulation program.

[1]J. Tomasi and M. Persico, Chem. Rev. (Washington, D.C.) **94**, 2027 (1994).
[2]M. Orozco and F. J. Luque, Chem. Rev. (Washington, D.C.) **100**, 4187 (2000).
[3]B. Roux and T. Simonson, Biophys. Chem. **78**, 1 (1999).
[4]P. A. Kollman, I. Massova, C. Reyes *et al.*, Acc. Chem. Res. **33**, 889 (2000).
[5]T. Takahashi, J. Sugiura, and K. Nagayama, J. Chem. Phys. **116**, 8232 (2002).
[6]M. S. Lee, J. F. R. Salsbury, and M. A. Olson, J. Comput. Chem. **25**, 1967 (2004).
[7]V. Barone, R. Improta, and N. Rega, Theor. Chem. Acc. **111**, 237 (2004).
[8]N. Rega, S. S. Iyengar, G. A. Voth, H. B. Schlegel, T. Vreven, and M. J. Frisch, J. Phys. Chem. B **108**, 4210 (2004).
[9]P. E. Smith and B. M. Pettitt, J. Chem. Phys. **95**, 8430 (1991).
[10]P. E. Smith and B. M. Pettitt, J. Chem. Phys. **105**, 4289 (1996).
[11]P. E. Smith, H. D. Blatt, and B. M. Pettitt, J. Phys. Chem. B **101**, 3886 (1997).
[12]P. H. Hunenberger and J. A. McCammon, J. Chem. Phys. **110**, 1856 (1999).
[13]M. Bergdorf, C. Peter, and P. H. Hunenberger, J. Chem. Phys. **119**, 9129 (2003).
[14]S. Bogusz, T. E. Cheatham III, and B. R. Brooks, J. Chem. Phys. **108**, 7070 (1998).
[15]S. Sakane, H. S. Ashbaugh, and R. H. Wood, J. Phys. Chem. B **102**, 5673 (1998).
[16]G. Hummer, L. R. Pratt, and A. E. Garca, J. Chem. Phys. **107**, 9275 (1997).
[17]W. F. van Gunsteren, S. R. Billeter, A. A. Eising, P. H. Hunenberg, P. Kruger, A. E. Mark, W. R. P. Scott, and I. G. Tironi, *Biomolecular Simulation: The GROMOS96 Manual and User Guide* (Hochschulverlag AG an der ETH Zürich, Zürich, 1996).
[18]W. D. Cornell, P. Cieplak, C. I. Bayly, and P. A. Kollman, J. Am. Chem. Soc. **117**, 5179 (1995).
[19]A. D. MacKerell, Jr, D. Bashford, M. Bellot *et al.*, J. Phys. Chem. B **102**, 3586 (1998).
[20]J. D. Jackson, *Classical Electrodynamics*, 3rd ed. (Wiley, New York, 1999).
[21]R. P. Bell, Trans. Faraday Soc. **27**, 797 (1931).
[22]L. Onsager, J. Am. Chem. Soc. **58**, 1486 (1936).
[23]H. L. Friedman, Mol. Phys. **29**, 1533 (1975).
[24]A. H. Juffer, E. F. F. Botta, B. A. M. van Keulen, A. van der Ploeg, and H. J. C. Berendsen, J. Comput. Phys. **97**, 144 (1991).
[25]W. C. Still, A. Tempczyk, R. C. Hawley, and T. Hendrickson, J. Am. Chem. Soc. **112**, 6127 (1990).
[26]J. Warwicker and H. C. Watson, J. Mol. Biol. **157**, 671 (1982).
[27]I. Klapper, R. Hagstrom, R. Fine, K. Sharp, and B. Honig, Proteins **1**, 47 (1986).
[28]S. Miertuš, E. Scrocco, and J. Tomasi, Chem. Phys. **55**, 117 (1981).
[29]R. Zauhar and R. Morgan, J. Mol. Biol. **186**, 815 (1985).
[30]P. Shaw, Phys. Rev. A **32**, 2476 (1985).
[31]Y. N. Vorobjev and H. A. Scheraga, J. Comput. Chem. **18**, 569 (1997).
[32]M. Cossi, G. Scalmani, N. Rega, and V. Barone, J. Comput. Chem. **117**, 43 (2002).
[33]G. Scalmani, V. Barone, K. N. Kudin, C. S. Pomelli, G. E. Scuseria, and M. J. Frisch, Theor. Chem. Acc. **111**, 90 (2004).
[34]H. J. C. Berendsen, J. P. M. Postma, W. F. van Gunsteren, and J. Hermans, in *Intermolecular Forces*, edited by B. Pullman (Reidel, Dordrecht, 1981).
[35]A. Laio and M. Parrinello, Proc. Natl. Acad. Sci. U.S.A. **99**, 12562 (2002).
[36]I. G. Tironi, R. Sperb, P. E. Smith, and W. F. van Gunsteren, J. Chem. Phys. **102**, 5451 (1995).
[37]T. Darden, D. York, and L. Pedersen, J. Chem. Phys. **98**, 10089 (1993).
[38]D. V. der Spoel *et al.*, *Gromacs User Manual version 3.0*, Nijenborgh 4, 9747 AG Groningen, The Netherlands, 2001.
[39]M. P. Allen and D. J. Tildesly, *Computer Simulation of Liquids* (Oxford University Press, Oxford, 1987).
[40]M. Pavone, G. Brancato, O. Crescenzi, and V. Barone (unpublished).
[41]M. Neumann, Mol. Phys. **50**, 841 (1983).
[42]H. E. Alper and R. M. Levy, J. Chem. Phys. **91**, 1242 (1989).
[43]D. van der Spoel, P. J. van Maaren, and H. J. C. Berendsen, J. Chem. Phys. **108**, 10220 (1998).
[44]K. Watanabe and M. L. Klein, Chem. Phys. **131**, 157 (1989).
[45]A. Amadei, G. Chillemi, M. A. Ceruso, A. Grottesi, and A. D. Nola, J. Chem. Phys. **112**, 9 (2000).